Determination of Thermomechanical Properties of a Model Polymer Blend

Brunero Cappella* and Senthil Kumar Kaliappan

Federal Institute for Materials Research and Testing (BAM), Unter den Eichen 87, D-12205 Berlin, Germany

Received August 17, 2006; Revised Manuscript Received October 20, 2006

ABSTRACT: Force−displacement curves have been acquired with an atomic force microscope (AFM) on a model polymer blend of polystyrene/poly(*n*-butyl methacrylate) (PS/PnBMA) as a function of temperature. A novel analysis technique, based on Hertz theory, permitted us to determine Young's modulus of PS and PnBMA, away from the interface (at distances larger than 1 mm) as well as close to the interface (at distances smaller than 80 μm) with a resolution of 800 nm. The inherent difference in the glass transition temperature of the polymers resulted in their different viscoelastic behavior. For the first time, it is possible not only to measure Young's modulus of the model blend components but also to map the morphology of the PS/PnBMA model blend based on Young's modulus of the constituting polymers as a function of temperature. Furthermore, differences between the thermomechanical properties of the polymers away from and in the vicinity of the interface can be characterized. This important topic can be addressed only with a tool able to measure local quantities, and not with measurements based on averages on a large ensemble of molecules, like dynamic mechanical analysis (DMA). The modulus of PnBMA and PS calculated from AFM force−displacement curves is in excellent agreement with the DMA and AFM data from our previous measurements.

Introduction

Nanomechanical measurements based on atomic force microscope (AFM) have made probing of surface mechanical properties with nanometer scale lateral and vertical resolution a reality. A number of successful measurements on polymers using this approach have been demonstrated to date.[1−5] The focus in recent studies was to investigate glass transitions in polymer films as most of the physical properties of a polymer depend on its glass transition temperature T_g.[6−8] For instance, the storage modulus of a polymer decreases by almost 3 orders of magnitude by going from the glassy state to the rubbery state. As AFM was shown to be able to determine the local mechanical properties of materials as a function of temperature with high lateral resolution,[9,10] the possibility to characterize complex structures that cannot be examined with other techniques, e.g., polymer blends and copolymer domains, is the current challenge in this field of microscopy.

Polymer blends of homopolymers are interesting for diverse reasons. First, mixing of polymers is interesting from a theoretical point of view, as it is of great importance to know the structure and morphology of the polymer blend and the influence of the morphology on the resulting blend properties. Second, polymer blends allow the optimization of some properties compared to that of isolated homopolymers, and hence they provide an economic way to create new materials with desired properties. The properties of the polymer blends are to a large extent determined by the morphology, i.e., the shape, size, and distribution of the components. Of all the properties of immiscible polymer blends, the interfacial properties between the two adjacent polymer phases are the least understood. The limited amount of information available about the polymer−polymer interface is a direct consequence of the fact that very few techniques allow one to study them directly.[11,12] Several techniques are useful in studies of polymer interfaces, but they provide only indirect information.[12−16]

Recently, a substantial amount of research work has been focused in mapping the morphology and composition of polymer blends and copolymers using AFM.[17] Some aspects of compositional identification are intrinsic to the AFM operation, as the interaction forces acting between tip and surface comprise of chemical information, and the sample indentation contains details about the viscoelastic properties of the sample. Novel imaging methods exploiting the tip−sample interaction forces have been recently implemented and are described in review articles.[18,19]

Friction force imaging and phase imaging are two of these techniques and are being used for compositional and morphological mapping of polymer films. In friction force imaging experiments, the cantilever is scanned perpendicular to its main axis and the torsion of the cantilever is measured. In the case of phase imaging, the phase shift between the cantilever driving signal and the cantilever's response is measured in tapping mode.[20] Both signals, i.e., torsion and phase shift, are due to a complex convolution of the tip−sample adhesion, the viscoelasticity and the sample topography.[21,22] Hence, while useful for providing image contrast, the tip−sample interactions producing cantilever's torsions and phase shift are not thoroughly understood, and the quantitative measurement of sample properties through such signals has not been achieved yet.

Force−displacement curves can be used both for image contrast and for the quantitative study of local variations of sample properties. To this aim, mechanical properties,[3,23] adhesion,[24−28] and specific forces[29,30] have been used. In this work, we have used force−displacement curves to investigate a model polymer blend of polystyrene/poly(*n*-butyl methacrylate) (PS/PnBMA) by characterizing its mechanical properties. Both polymers used in this study have been previously investigated using AFM.[9,10] In both cases, force−distance curves have been acquired at different temperatures and frequencies. Diverse mechanical quantities, e.g., Young's modulus, have been

* Corresponding author. E-mail: Brunero.Cappella@bam.de. Telephone: +49 30 8104 3343.

10.1021/ma061896g CCC: $33.50
Published on Web 12/19/2006

calculated for each temperature and frequencies. The effect of frequency and temperature on the calculated mechanical quantities has been equated by means of the time−temperature−superposition principle. Following this method, isotherms of a certain quantity, i.e., curves containing the given quantity at different frequencies, but at the same temperature, are shifted until they overlap with a reference isotherm. The obtained shift factors can be fitted with two equations, the Williams−Landel−Ferry (WLF) or the Arrhenius equation, depending on whether the experimental temperatures are larger or smaller than T_g. Such an experimental procedure allowed us to characterize the viscoelastic behavior of PnBMA and to quantitatively determine its elastic properties in agreement with dynamic mechanical analysis (DMA) measurements.[9] In the case of PS, T_g has been measured as the temperature at which the WLF and the Arrhenius fit of the shift factors intersect.[10]

A previous study by Kim et al. on the interaction energies for PS/PnBMA blends with varying molecular weights has shown that blends containing PS and PnBMA are immiscible at high molecular weights.[31] Hence, the two polymers were found to be a suitable model for the study of elastic-plastic properties of polymer blends.

Having shown in our previous works that AFM force−displacement curves are able to determine the mechanical properties of polymers as a function of temperature, we focused the present work on the determination of micrometer scale local properties of polymers, i.e., on the influence of morphology on the mechanical properties of a model polymer blend in the vicinity of the interface. The ultimate objective is to extract the mechanical properties of the blend components as a function of temperature, and thereby to characterize the morphology of the model blend. Emphasis is put on the elastic region of the force−displacement curve. Hertz theory,[32] coupled with a novel method[9,10] that takes into account also plastic deformations, has been used for the analysis of the force−displacement curves.

Experimental Section

PnBMA was obtained from Scientific Polymer Products Inc. (Ontario, NY), and it was used without any further purification. The molecular weight, the polydispersity index, and the glass transition temperature as provided by the supplier are M_w = 319 kDa, $M_w/M_n \leq 2.58$, and T_g = 22 °C. PS was purchased from BDH Chemicals Ltd. (Poole, England). The molecular weight, the polydispersity index, and the glass transition temperature as reported are M_w = 100 kDa, $M_w/M_n \leq 2$, and T_g = 100 °C.

The sample preparation has been carried out in three steps. First films of PnBMA and PS were obtained by melting the individual polymers between the dual spring loaded glass slides in vacuum at 140 and 200 °C respectively. The glass slides have been heated from below by means of a 340-temperature controller (Lake Shore Cryotronics, Westerville, OH). The pressure applied on the glass slides during the melting ensures that the films are uniformly thick and the surfaces are flat. Successively, the films were cut in two 1 cm^2 large square films. As a last step, the model PS/PnBMA blend was prepared. To this aim, the PnBMA film was placed on top of the PS film between the two glass slides of the dual spring loaded system and PnBMA was molten again at 140 °C, as shown in Figure 1a. Because of the applied pressure, molten PnBMA flowed down and formed the PS/PnBMA interface along the edges of the PS film, as indicated by the arrows. The bottom side of the sample facing the heater was used for measurements. The cross section of the sample is shown at the bottom of Figure 1b.

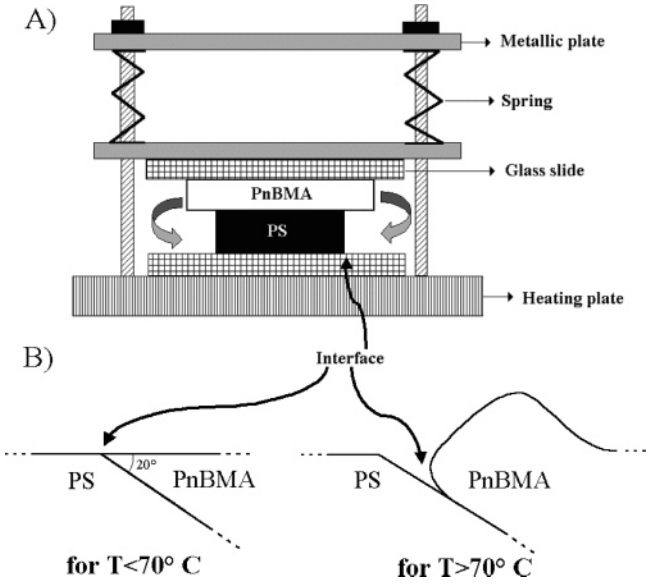

Figure 1. (a) Graphical representation of the dual spring loaded glass slides used in preparing the model polymer blend samples. Pressure has been applied on the polymer films by the dual spring loaded arrangement. The polymer films are heated by means of a temperature controller on the bottom. (b) Schematic cross section of the model blend sample prepared from the polymer melts at temperatures below 70 °C (the sample shows no topographical variations between the two phases) and above 70 °C, where the PnBMA phase has enough energy to dewet the PS phase by forming a large and deep groove running parallel to a high pile. The angle of cut, i.e., the angle formed by the bottom and the lateral faces of the PS phase, has been measured and it is 20 ± 5°.

Previous to the preparation of the model blend, the edges of the PS film have been imaged in tapping mode, in order to determine the angle of cut, i.e., the angle formed by the bottom and the lateral faces. This has resulted to be 20 ± 5°, as shown in the left part of Figure 1b. The PS/PnBMA model blend film was relatively thick (≈200 μm) and thereby allowed us to perform large indentations without artefacts due to the large stiffness of the substrate.[33] In order to avoid such artefacts, indentation depths should not exceed 10% of the film thickness.[34] The topography of 80 × 80 μm^2 areas at the interface has been acquired in tapping mode after each measurement at various temperatures. At some temperatures and in some parts of the interface the PS and the PnBMA phases are separated by a small step, in the order of few tenths of nanometer, but in most cases it was not possible to point out the interface, as there were no topographical discontinuities between the PS and the PnBMA phases. In general, the surface of PS was flatter and smoother in comparison with the surface of PnBMA.

AFM force−displacement curves were acquired using a MFP 3D microscope (Asylum Research, Santa Barbara, CA). Point-probe NCL cantilevers (Nanosensors, Germany) with a spring constant of k_c = 45 N/m was used to acquire all the force−displacement curves. The spring constant has been measured from the noise spectrum of the cantilever.[18] When the spring constant of the cantilever is less than the elastic modulus of the probed surface, then the force−distance curves will basically measure the cantilever's stiffness. On the other hand, a too high spring constant of the cantilever results in a bad force resolution.[18]

A metallic disk at the base of the polymer was heated using a 340-temperature controller. The surface temperature of the sample was measured using a PT100 fixed directly on the polymer surface. The surface temperature was allowed to equilibrate overnight and the temperature remained constant for several days (±0.3 °C on the surface). Force−displacement

curves were with high sampling density acquired over a range of temperatures from 32 to 70.1 °C over 38.5, 45, 51.4, 57.4, and 63.6 °C. Since the minimum step of the vertical piezo displacement is 1 pm and the piezoactuator acts like a capacitor, the piezoactuator displacement has been assumed to be continuous, and the probe rate is the frequency of the piezoactuator displacement, i.e., the frequency of the force−displacement curve. All the force−displacement curves were obtained at 1 Hz.

For each measurement at a particular temperature on PnBMA and PS, two sets of 100 force−displacement curves have been obtained at a distance of about 2 mm from the interface both on PnBMA and PS. Each set was acquired on different areas of the sample (usually $80 \times 80\ \mu m^2$) in force-volume acquisition mode. In force-volume mode, all the force−displacement curves start at a fixed height; an approach−withdrawal cycle is performed, then a lateral displacement away from the surface, again an approach−withdrawal cycle, and so on. In the case of measurements across the model PS/PnBMA interface, 10000 force−displacement curves have been acquired on an area of $80 \times 80\ \mu m^2$ in force-volume acquisition mode. All the force−displacement curves were triggered to reach a fixed maximum cantilever deflection of 400 nm, i.e., a maximum applied force of 18 μN. In total, more than 73000 curves have been taken into account for the analysis. Measurements have been carried out also on another PS/PnBMA model blend (sample II), but only Young's moduli away from the interface have been shown for comparison with the measurements on sample I and to prove the repeatability of the measurements.

Results and Discussion

The interaction between cantilever's tip and sample produces a cantilever deflection δ_c, measured with an optical lever deflection system. The applied force F is given by

$$F = k_c \delta_c \tag{1}$$

where k_c is the spring constant of the cantilever.

Along the contact curves the sample deformation D due to tip−sample interaction is given by

$$D = Z - \delta_c \tag{2}$$

where Z is the piezo displacement. According to the Hertz theory,[32] the applied force and the sample deformation are related as

$$F = k_c \delta_c = E_{tot} \sqrt{R} D^{3/2} \tag{3}$$

where R is the tip radius and E_{tot} is defined by

$$\frac{1}{E_{tot}} = \frac{3}{4}\left(\frac{1-\nu^2}{E} + \frac{1-\nu_t^2}{E_t}\right) \tag{4}$$

where ν_t, ν, E_t and E are the Poisson's ratios and Young's moduli of tip and sample. If E_t is much larger than E, we can write $E_{tot} = 4E/3(1-\nu^2)$ and

$$D^{3/2} = \frac{3(1-\nu^2)}{4} \frac{1}{E} \frac{k_c}{\sqrt{R}} \delta_c \tag{5}$$

The proportionality between $D^{3/2}$ and the applied force, obtained in eq 5, is predicted by all other continuum contact theories, provided the forces are shifted by a factor depending on the adhesion between tip and sample.[35] When the adhesive force is much smaller than the applied force, its influence on the resulting Young's modulus becomes smaller and when modeling approach contact curves the effect of adhesion can be neglected.[36] To this aim, the relevant adhesion is the one measured in curves where only elastic deformations take place.

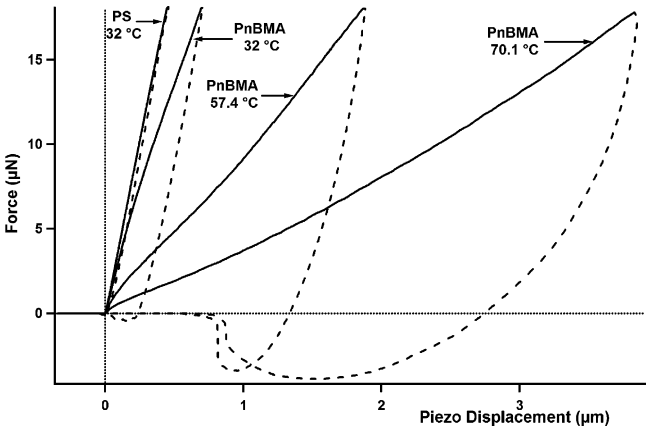

Figure 2. Approach (continuous solid line) and withdrawal (broken line) force−displacement curves acquired on PS at 32 °C and on PnBMA at 32, 57.4, and 70.1 °C. Hysteresis and plastic deformation increase with increasing temperature for curves acquired on PnBMA. In the case of PS, there are no large variations in hysteresis and plastic deformation with increasing temperature.

Figure 2 shows the approach (continuous solid line) and the withdrawal (broken line) curves acquired on PnBMA at 32, 57.4, and 70.1 °C and on PS at 32 °C. The force−displacement curves acquired on the model blend present a yielding point.[5] The yielding force is a critical force $F_{yield} = k_c \delta_{yield}$ at which the polymer starts to undergo plastic deformations and the measured stiffness decreases, and can be seen as a kink in the approach contact curve. Moreover, when $F_{max} > F_{yield}$, as a consequence of plastic deformations, the retraction contact curve does not overlap the approach contact curve, as seen in all the force−displacement curves on PnBMA in Figure 2. The area between the approach and the withdrawal contact curves above $F = 0$ is called the hysteresis of the force−displacement curves. Hysteresis is a direct measure of the energy that has been dissipated within the sample because of plastic deformations and the plastic deformation δ_p is defined as the intercept of the withdrawal contact curves with the axis $F = 0$.[18] The curves acquired on PnBMA show a large increase of the hysteresis and of the plastic deformation with temperature. On the other hand, the force−displacement curves obtained on PS at various temperatures overlap each other. Also, the hysteresis and the plastic deformation of PS are much smaller than those of PnBMA at all temperatures. Such a difference in the behavior of the polymers is due to their different T_g. Since all experimental temperatures are higher than T_g of PnBMA (22 °C), PnBMA is in its glass−rubber transition region, and an increase in temperature results in a decrease of the stiffness of the polymer. As a consequence, PnBMA can be plastically deformed at relatively small forces, thus dissipating more energy. Whereas, the T_g of PS is 100 °C and PS is in its glassy state at all experimental temperatures. Hence, the stiffness of PS remains nearly constant by increasing the temperature and both the plastic deformation and the dissipated energy remain constant and smaller than in the case of PnBMA.

For a quantitative determination of mechanical properties it is necessary to analyze the $D^{3/2}(\delta_c)$ functions ($D^{3/2}$ curves). Figure 3 shows the average of 100 $D^{3/2}$ curves, calculated from the approach contact curves, obtained on PnBMA far from the interface at 45 °C. The curves present two distinct linear regions

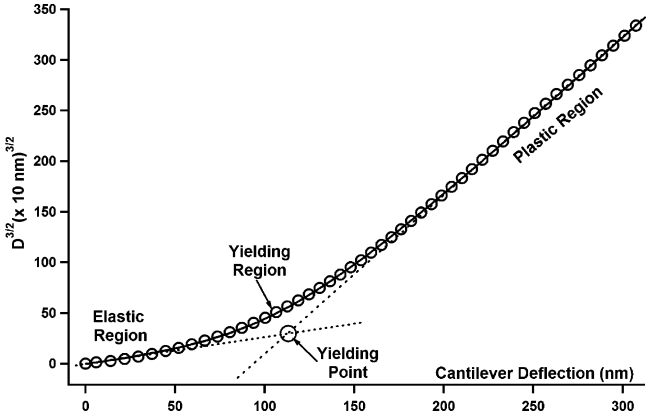

Figure 3. Fit of an average $D^{3/2}$ vs cantilever deflection curve (empty circles), acquired on PnBMA away from the interface at 45 °C, with a hyperbola (solid line). The two linear regimes ($\delta_c \ll \delta_{yield}$ and $\delta_c \gg \delta_{yield}$) are represented as dotted lines and the intersection of these lines (circle) gives the yielding point δ_{yield}. For the sake of clarity only one in ten points on the curve up to $\delta_c \approx 300$ nm is shown here.

connected by a nonlinear one, where the value of the slope of the first linear region increases to the value of the second one.[9,10] The first region is the elastic regime of the deformation, the nonlinear region represents yielding of the polymer, and the slope of the second linear region is always larger than that of the first one. The slope of the linear regions is inversely proportional to the stiffness of the polymer (see eq 5). Therefore, the polymer has become more compliant after yielding. On plastically indenting a polymer, some of the polymer chains are squeezed out of the bulk and piled up adjacent to the tip. Displacement of such groups of chains makes it easier for the tip to penetrate the sample. In other words, the resistance of the sample to being deformed, i.e., the stiffness, decreases.[37] Hence, such a decrease in stiffness after yielding is the expected behavior for AFM indentations at $F_{max} > F_{yield}$. We define the yielding point as the intersection of the two straight lines, represented by a circle in Figure 3. If the polymer chain length, entanglements, and the stress in the contact area were uniform, the yielding point would be exactly a point and the $D^{3/2}$ curve would compose of two lines intersecting at $\delta_c = \delta_{yield}$. However, the stress in the contact area and the chain length and entanglements are not uniform and hence there is a distribution of yielding points leading to the nonlinear region in the $D^{3/2}$ curve.

The measured $D^{3/2}$ curves have been fitted with a hyperbola in the form:[9]

$$D^{3/2}(\delta_c) = (\beta\delta_c - \epsilon) + \sqrt{\alpha^2\delta_c^{\,2} - 2\epsilon(\beta - \gamma)\delta_c + \epsilon^2} \quad (6)$$

with $\alpha > 0$, $\beta > 0$, $\gamma > 0$, $\epsilon > 0$, and $\beta - \alpha < \gamma < \beta + \alpha$.

In the two linear regions $\delta_c \ll \delta_{yield}$ and $\delta_c \gg \delta_{yield}$, where $D^{3/2}$ is proportional to δ_c, the hyperbola can be approximated with two lines, i.e., its tangent at $\delta_c = 0$ and its asymptote for $\delta_c \to \infty$, whose equations are given by:[9]

$$\begin{cases} \delta_c \ll \delta_{yield} \Rightarrow D^{3/2} \cong \gamma\delta_c \\ \delta_c \gg \delta_{yield} \Rightarrow D^{3/2} \cong (\beta + \alpha)\left[\delta_c - \dfrac{\epsilon}{\alpha}\left(1 - \dfrac{\gamma}{\alpha + \beta}\right)\right] \end{cases} \quad (7)$$

and δ_{yield}, defined as the intersection of the two lines, is given by

$$\delta_{yield} = \epsilon/\alpha \quad (8)$$

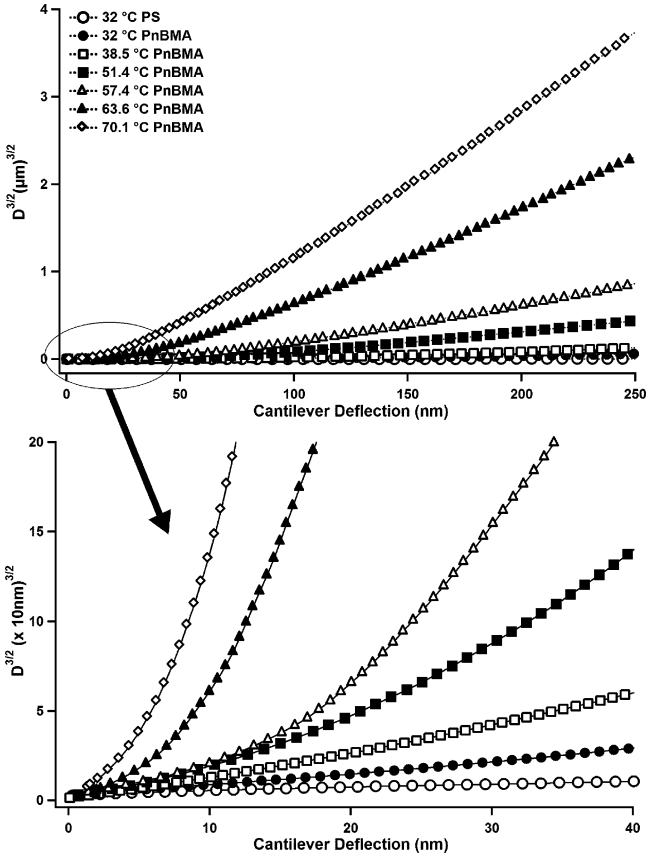

Figure 4. Average $D^{3/2}$ curves at various temperatures (32, 38.5, 51.4, 57.4, 63.6, and 70.1 °C) on PnBMA and at 32 °C on PS. All curves are calculated from force volumes acquired away from the interface. The top portion of the figure shows the curves up to $\delta_c \approx 250$ nm, and the bottom part up to $\delta_c \approx 40$ nm, so that the elastic region can be seen more clearly. The slope of the two linear regimes ($\delta_c \ll \delta_{yield}$ and $\delta_c \gg \delta_{yield}$) increases with increasing temperature for PnBMA, as PnBMA is above its glass transition temperature.

It is important to note that this model treats the yielding region as a transition from the first elastic deformation to a second deformation with a lower stiffness. Thus, a plastically deformed polymer can be treated, only from a mathematical point of view, as an elastically deformed polymer with a smaller stiffness, by changing the origin of the $D^{3/2}$ curves from the point [0,0] to the point [δ_{yield}, $D^{3/2}(\delta_{yield}) = \gamma\epsilon/\alpha$].

Figure 4 contains the average $D^{3/2}$ curves obtained at 32, 38.5, 51.4, 57.4, 63.6, and 70.1 °C on PnBMA far from the interfacial region. Panel b in Figure 4 puts in evidence the elastic regime of the curves. Only the average $D^{3/2}$ curve obtained at 32 °C on PS far from the interface is shown here, as the $D^{3/2}$ curves on PS, like the force−distance curves, overlap each other at all measured temperatures. One can immediately note that the slope of the two linear regimes in the $D^{3/2}$ curves increases with increasing temperature for the curves acquired on PnBMA. This is again due to the fact that PnBMA is in the glass−rubber transition region, where Young's modulus of the polymer decreases by almost 3 orders of magnitude. This decrease in Young's modulus is the reason for the increase in the slopes of the curves in the elastic regime (see eq 5). Whereas, no variations can be seen in the $D^{3/2}$ curves on PS, since PS is in its glassy state, and Young's modulus of a glassy polymer fairly remains a constant.

The effect of temperature and frequency on the yielding force and on Young's modulus E can be quantitatively determined.[9,10] As already shown, following the Hertz theory, for $\delta_c \ll \delta_{yield}$

$$E \cong \frac{3(1-\nu^2)}{4}\frac{k_c}{\sqrt{R}}\frac{1}{\gamma} \tag{9}$$

where γ is the slope of the linear elastic regime of the $D^{3/2}$ curve for $\delta_c \rightarrow 0$. The Poisson's coefficient ν of the sample has been assumed to be 0.33, which is a common value for polymers. It is important to note that, because of the distribution of yielding points, the stiffness of the polymer after yielding influences also the stiffness in the elastic region, i.e., before yielding. As the temperature increases, the yielding points become smaller and smaller, and some groups of chains yield also for very small loads. Hence, the influence of the stiffness in the plastic regime on the stiffness in the elastic regime becomes larger and larger with increasing temperature. As a matter of fact, a correct measure of the stiffness in the elastic region and of Young's modulus requires the quantitative determination of the stiffness also in the plastic region.[9] This is the reason why we have acquired long force−distance curves with large plastic deformations, even if we focus the analysis on the elastic regime of deformations.

The knowledge of the cantilever's spring constant k_c and of the tip radius R is also fundamental in calculating Young's modulus using AFM. The spring constant has been measured from the noise spectrum of the cantilever[18] and is $k_c = 45$ N/m. The tip radius has not been measured, rather it has been chosen so that the calculated Young's modulus of PnBMA matches Young's modulus of PnBMA measured using DMA in our previous experiment.[9] For $R = 30$ nm there is a good agreement between Young's modulus obtained using DMA and AFM techniques. Such a value of the tip radius is only a rough approximation and compensates some of the errors due to the approximation of the tip as a spherical tip and to the fact that in the Hertz model adhesion is neglected.

Figure 5 shows the logarithm of Young's modulus vs temperature obtained in several measurements. The different plots are as follows:

1. Present measurement, PnBMA (empty circles) and PS (empty squares), far from the interfacial region;

2. Present measurement on another PS/PnBMA model blend (sample II), far from the interfacial region; only Young's modulus of PnBMA is shown (empty triangles);

3. Previous AFM measurements, PnBMA (filled circles) and PS (filled squares) (see refs 9 and 10, respectively);

4. DMA measurement on PnBMA (solid line) (see ref 9).

There is a very good agreement between the present AFM measurements on one side and the previous experiments and the DMA data on the other side. Such a good agreement is particularly remarkable when considering the several fundamental differences between the measurements:

1. The four AFM measurements (PnBMA, PS, model blend I and model blend II) have been performed with four different cantilevers, i.e., different tips with different radii.

2. As already explained, Young's modulus of both polymers was obtained in our previous experiments by acquiring force−distance curves at different frequencies and taking advantage of the time−temperature superposition principle and of WLF and/or Arrhenius equation;

3. in our previous measurements films were cast from concentrated polymer solutions, whereas in this work films were obtained by melting the polymers in vacuum between two glass plates.

The significant agreement between the calculated Young's modulus of PnBMA and PS from different experiments proves the repeatability of the measurements and the accuracy of our analysis technique used to calculate Young's modulus.

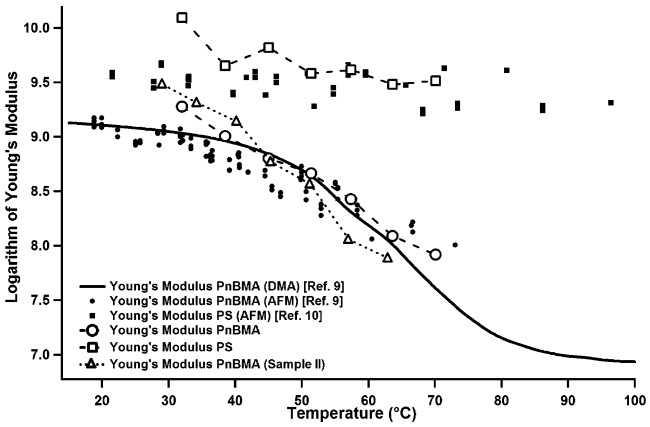

Figure 5. Log(E) of PnBMA (empty circles, sample I, and empty triangles, sample II) and PS (empty squares) calculated from the $D^{3/2}$ curves obtained away from the interface in comparison with log(E) of PnBMA (filled circles) and PS (filled squares) determined in our previous AFM experiments.[9,10] Also log(E) of PnBMA measured by means of DMA in a previous experiment (see ref 9) is shown (thick continuous line). The calculated Young's moduli are in very good agreement with each other.

In the present experiment, the logarithm of Young's modulus of PnBMA decreases from about 9.2 (1.9 GPa) at 32 °C to about 7.9 (82 MPa) at 70.1 °C. Again, Young's modulus of PnBMA decreases by more than 1 order of magnitude because PnBMA is in the glass−rubber transition region over the entire experimental temperature range. In comparison, it is clear that there are only small variations in Young's modulus of PS with increasing temperature, since PS is in the glassy state.

It can be noted from Figure 5 that at low temperatures Young's modulus of molten PnBMA away from the interface is clearly higher than Young's modulus of the solvent cast PnBMA,[9] both on sample II (empty triangles, up to 40.3 °C) and on sample I (empty circles, only at 32 °C). Starting from 45.4 °C for sample II and from 38.5 °C for sample I, Young's modulus of PnBMA is in good agreement with the previous AFM and DMA data. In the case of PS, Young's modulus of the molten polymer is always higher than that of the solvent cast one.[10] As already explained, in order to prepare the model blend, PS and PnBMA films were pressed against each other between glass slides and melted. By applying pressure on the glass slides during the melting and cooling processes of film preparation, internal stresses are likely to be induced within the films. The residual stresses could be removed by heating the unconstrained sample above the T_g of PS, holding it at that fixed temperature for few hours, and finally cooling at a very low rate. However, this process would induce PnBMA to move and accumulate away from the intended PS/PnBMA interface, as the two polymers are inherently immiscible.[31] This would result in undesirable topographical modifications at the interfacial region. We attribute the higher values of Young's modulus of the molten polymers at low temperatures to the effect of amounts of residual solvent still present in the solvent-cast samples and primarily to the additional stresses induced during sample preparation. In PnBMA the induced stresses can be relaxed with time at temperatures above its T_g (22 °C), whereas the PS chains do not have enough thermal energy and time to relax such stresses.

After the determination of Young's modulus of both polymers far away from the interface, necessary to assess the repeatability and the accuracy of our measurements, we turn to the main

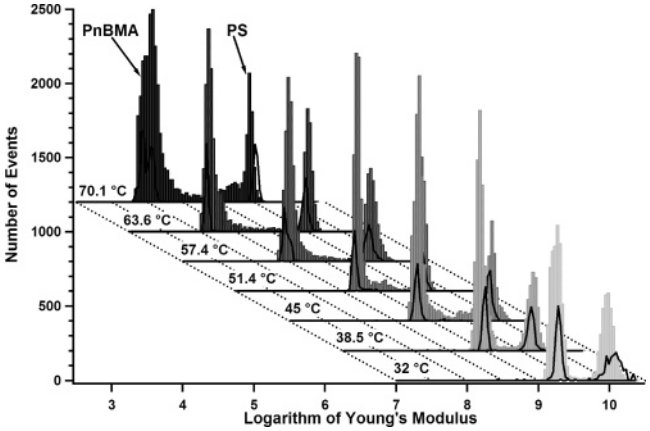

Figure 6. Histograms of log(E) for the measurements in 80 × 80 μm^2 areas across the PS/PnBMA interface (bars) and log(E) of PnBMA and PS away from the interface (solid lines). The histograms have been shifted both horizontally and vertically for clarity. The peak on the left (right) hand side corresponds to log(E) of PnBMA (PS).

issue of the present work, i.e., the characterization of the mechanical properties of the polymers in the vicinity of the interface. We remind once again that our measurements, and in general AFM force-volume measurements do not represent a characterization of the mechanical properties of the model blend in the interfacial region, since the interfacial region between two immiscible polymers, being in the order of some nanometers, is well under the resolution of force-volume measurements, roughly given by twice the tip radius, i.e., 30−100 nm. Our measurements represent rather a local measurements in the micrometer scale.

Young's modulus of PS/PnBMA model blend is calculated from the fit parameter γ of the $D^{3/2}$ curves for each set of 10000 force−displacement curves acquired in an 80 × 80 μm^2 area across the interface (see eq 9). Figure 6 represents the histograms of log(E) obtained from the measurements across the PS/PnBMA interface (bars) together with histograms of log(E) of PnBMA and PS away from the interface (solid lines). The histograms have been shifted both horizontally and vertically for clarity with the histogram at 32 °C as reference. The measurement at 70.1 °C is the sum of two histograms, as Young's modulus of PnBMA close to the interfacial region did not reach the value far from the interface, and a second force volume measurement has been made on an adjacent 80 × 80 μm^2 area.

The peak on the left-hand side of each histogram represents Young's modulus of PnBMA and the peak on the right-hand side is Young's modulus of PS. Once again, it can be noted that Young's modulus of PS varies very little in comparison to Young's modulus of PnBMA, which decreases by more than 1 decade.

A first important feature of Young's modulus of both polymers is that the histograms obtained away from the interface overlap the ones measured close to the interface. On a closer look, one can also note that the histograms on PS at the interface have a Gaussian shape, whereas the histograms on PnBMA at the interface present a shoulder on the right-hand side. This means that Young's modulus of PnBMA at the interface is higher than Young's modulus of PnBMA away from the interface.

In order to link mechanical properties and morphology of the sample, it is necessary to map the calculated Young's modulus. Figure 7 shows gray scale images of Young's modulus obtained across the interface for all temperatures. Black (white) corresponds to the least (maximum) Young's modulus. In order to visualize the effect of temperature on Young's modulus, all images are shown with the same gray scale.

The PnBMA phase becomes darker with increasing temperature as a result of the decrease in Young's modulus. Since PS is in the glassy state, the parts of the images on PS do not show noteworthy changes. The transition between Young's modulus of the two polymer phases is sharp and allows one to point out the interface precisely, with a resolution of ca. 800 nm. Thus, it is possible to map the morphology of the polymer model blend based on Young's modulus of its constituting polymers.

The transition between the two phases can be observed more in detail in Figure 8, showing the averaged line profiles of log(E) across the interfacial region at all temperatures. The line profiles have been shifted horizontally so that they all start to decrease from the PS value to the PnBMA value at the same point. First of all, it can be noted that the plateau values representing log(E) of PS are bunched together on the left-hand side of the graph for all temperatures, whereas log(E) of PnBMA decreases with increasing temperature. This is a further confirmation of the different viscoelastic properties of the two polymers due to their different T_g. Second, Young's modulus of PS is fairly constant at each temperature until the interface, while Young's modulus of PnBMA depends on the distance from the interface. In particular, with increasing distance from the interface, E decreases from the value on PS to the value on PnBMA away from the interface, indicated by the arrows on the right-hand side of the image. The distance at which the value of E on PnBMA away from the interface is reached, and hence the width of the region where Young's modulus of PnBMA depends on the distance from the interface, increases with increasing temperature. Nevertheless, the value on PnBMA away from the interface is reached at each temperature except at 70.1 °C. In this case it has been necessary to acquire a second force volume on an 80 × 80 μm^2 area adjacent to the first one. The second line profile, not shown here for clarity, matches the value of log(E) away from the interface.

We call the region where Young's modulus of PnBMA is a function of the distance from the interface "transition region". We would like to bring forward to the reader that the "transition region" we describe here is not identical with the transition region commonly associated with the interface between two polymers. The transition region revealed by our experimental data is several micrometers wide and is defined by the gradient of Young's modulus of the sample, whereas the transition region (in the common sense) is of the order of some nanometers for immiscible polymers and of some hundreds of nanometers for miscible polymers and is defined primarily by the gradient of the composition of the sample. As already remembered, PS and PnBMA are immiscible, and the width of the interfacial or transition region is on the order of 5 nm. Hence, changes in Young's modulus of PnBMA persisting over so many micrometers of distance cannot be caused by the presence of the PS/PnBMA interface. The long-range transition region of Young's modulus is caused by other effects that will be discussed in the following.

Before considering in detail the profiles of log(E) at various temperatures, let us discuss the possibility of characterizing the morphology of the model blend using Young's moduli of the constituting polymers. Figure 9a shows the profiles of log(E) = 9.48 (dark red line), down to log(E) = 9 (light yellow line), in steps of 0.08 (lines of increasing brightness, very close to each other and bunched together at the interface). Also the profiles of log(E) = 8.6 (green line) and of log(E) = 8.5 (blue line) are shown. The profiles are superimposed on the topo-

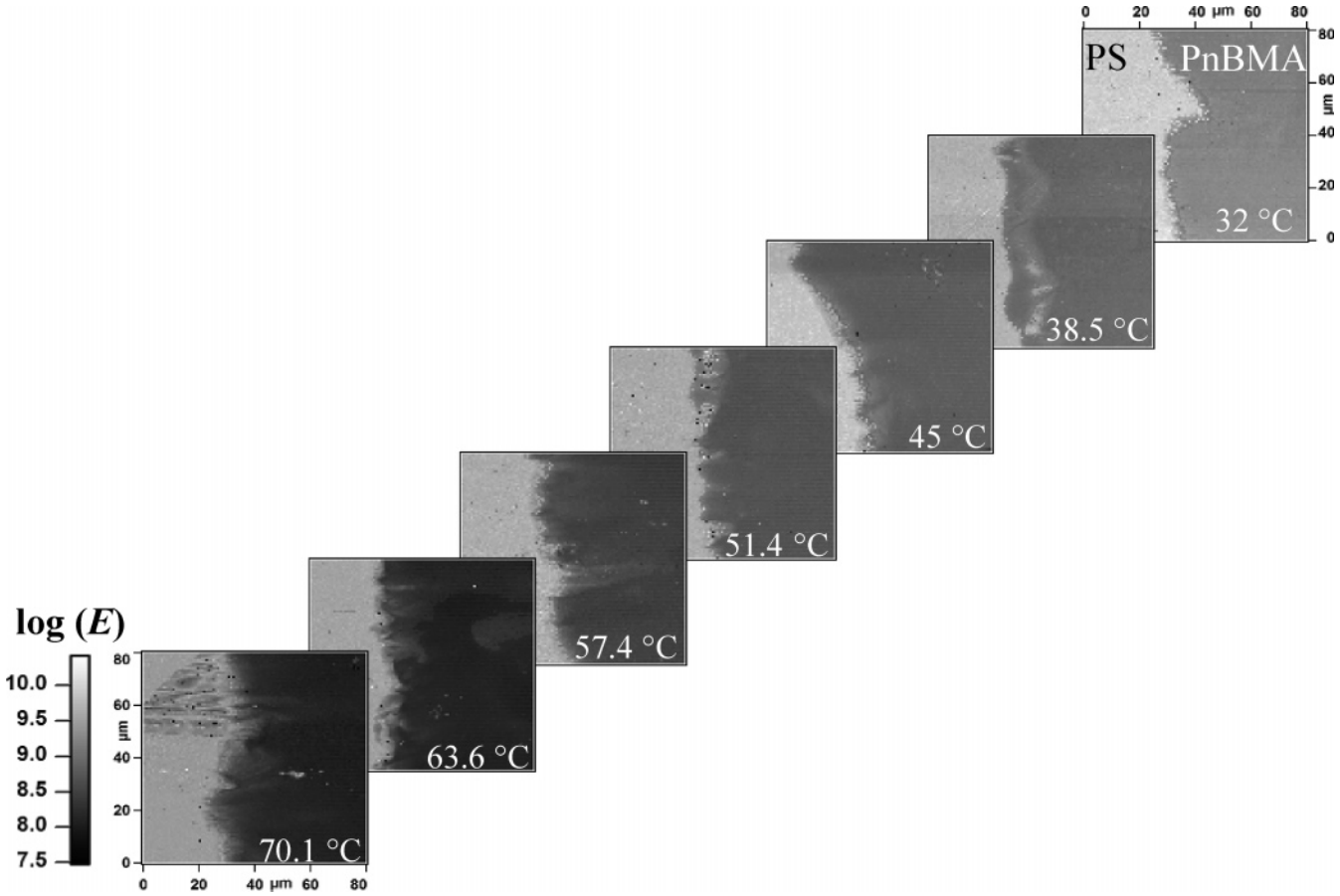

Figure 7. Images of log(E) obtained from the measurements on 80 × 80 μm^2 areas across the PS/PnBMA interface at various temperatures as indicated in the image. All the images have the same gray scale.

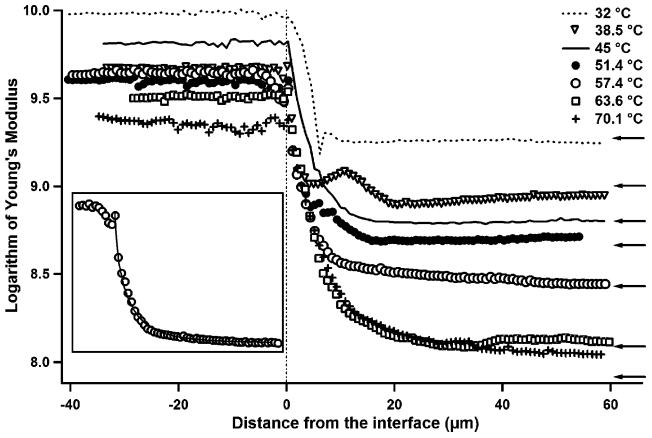

Figure 8. Averaged line profile of log(E) across the interface at all temperatures, calculated from the measurements shown in Figure 6. The line profiles have been shifted horizontally so that all line profiles starts to decrease at the same point. The inset shows the line profile of the modulus at 57.4 °C together with the profile calculated by assuming that deformations are described by the Tsukruk equation (eq 10) and that the underlying PS has a linear profile.

graphic image across the interface (gray image) at 57.4 °C. It can be seen that the profiles at the different values of log(E), defining the morphology of the model blend, strictly follow the interface, except the ones at log(E) = 8.6 and at log(E) = 8.5. As a matter of fact the two phases can be distinguished in the topographical image, acquired after the force volume, only thanks to the plastic deformations created during force−volume. Such deformations remain permanent on PS, whereas they can be relaxed with time on PnBMA, as PnBMA is in the glass−rubber transition region. Figure 9b represents the line profiles of the topography and of log(E) at the same position at 57.4 °C. The topography exhibits no discontinuity at the interface (dotted line perpendicular to the x-axis), that can be pointed out only with the help of the Young's modulus profile. A very important inference of such a plot is that the topographic variations do not influence the calculated Young's modulus.

We have already observed in Figure 8 the presence of a transition region, where Young's modulus increases from that of PnBMA to that of PS. As already pointed out, the stiffening of PnBMA several micrometers away from the interface cannot be explained by the presence of the some nanometers wide interfacial region, and must be rather related to geometrical constraints of the polymer in the several micrometer wide region near the interface. Even if not directly connected to the presence of an interface and to the composition of the sample, these phenomena are very relevant in characterizing the mechanical properties of blends of immiscible polymers, and we would like to discuss in the following some of the possible causes of such a stiffening of PnBMA at the boundary to PS.

One of the reasons for the stiffening of PnBMA in this region is the presence of macroscopic stresses developed in PnBMA in a several micrometer wide region near the PS/PnBMA interface, analogous to the ones causing the stiffening of PnBMA away from the interface at low temperatures (see text referring to Figure 5). The PnBMA phase tries to separate from the PS phase (dewetting) in order to reduce its surface free energy. PnBMA chains have more free volume in comparison to PS chains, as PnBMA is above its T_g. Thus, PnBMA has relatively more freedom of movement and can relax and increase its volume due to thermal expansion. The expansion and relaxation can occur, except at low temperatures, away from the interface,

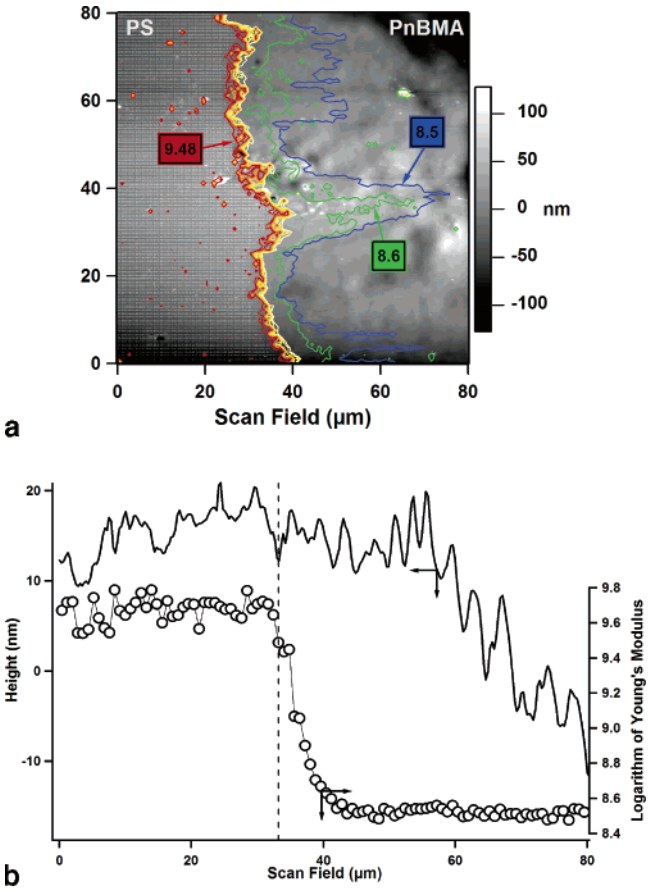

Figure 9. (a) Topographic image (gray scale) of the model blend at the interface at 57.4 °C and superimposed profiles of log(E) = 9.48 (dark red line), down to log(E) = 9 (light yellow line), in steps of 0.08 (lines of increasing brightness, very close to each other and bunched together at the interface). Also the profiles of log(E) = 8.6 (green line) and of log(E) = 8.5 (blue line) are shown. (b) Line profile of the topography (referred to left axis) and of log(E) (referred to the right axis) of the model blend across the interface. It can be seen that there is no discontinuity in the topography at the interface and also that the topography does not influence the determined Young's modulus.

because PnBMA is not subjected to geometrical constraints. On the contrary, expansion and relaxation cannot occur at the boundary to PS, since PnBMA is geometrically restricted by the presence of a relatively stiff polymer, for which PnBMA shows no affinity to mixing. In other words PS, being immiscible with PnBMA and having a relatively high stiffness at all experimental temperatures, acts like a hard wall or a solid and represents a geometrical constraint for the movement and the expansion of PnBMA. The expansion of PnBMA and its tendency to dewet the PS phase, together with the presence of a nearly solid boundary at the interfacial region induces stresses in the PnBMA phase.

Such an hypothesis of expansion-induced stresses is confirmed by the dramatic changes of the sample topography, accompanied by enormous stresses, above 70.1 °C, as PnBMA has enough thermal energy to dewet PS and to form a phase separated from PS by a large (≈30 μm) and deep groove (>6 μm), running parallel to a several micrometers high pile, as shown in the right part of Figure 1b. Such a change of the topography of the model blend made it impossible to carry out the experiment at temperatures higher than 70.1 °C.

Another plausible reason for the increase in Young's modulus of PnBMA over some tens of micrometers from the interface could be the effect of any underlying PS forming a double-layer sample. Since PS has a higher Young's modulus, any underlying PS would increase Young's modulus of PnBMA close to the boundary. The determination of the mechanical properties of double-layer samples is a disputed topic. To date, the most useful empirical equation taking into account the effect of a stiff substrate on the mechanical properties of a film on top of it is the one of Tsukruk,[39] giving the deformation D in the following form:

$$\frac{D}{D_H} = \sqrt[4]{\frac{J^{4/3} + 0.8t/\sqrt{RD_H}}{\sqrt{1 + (0.8t/\sqrt{RD_H})^2}}} \qquad (10)$$

Here D_H is the Hertz deformation that would be obtained on the top film without substrate, t is the thickness of the top film, and $J = E_f/E_s$ is the ratio of Young's moduli of the top film E_f and of the substrate E_s.

The inset in Figure 8 shows again the profile of log(E) across the interface at 57.4 °C superimposed on the profile calculated assuming that deformations are described by the Tsukruk equation (eq 10) and that the underlying PS has a linear profile. The angle of inclination of the underlying PS has been adjusted in order to match the measured profile and is found to be 2°. This means that the presence of underlying PS would influence Young's modulus of PnBMA to such an extent only if the inclination angle were very small or, in other words, only if the PnBMA film on top of it were very thin. On the contrary, as already said and shown in Figure 1b, the angle of inclination at the edge of the PS film that we measured is 20 ± 5°. Hence, since our lateral resolution in a force volume map is 800 nm, already after one point from the interface, i.e., from the PS edge, the thickness of PnBMA is about 300 nm. On the other hand, at 57.4 °C the maximum elastic deformation achieved on PnBMA at a distance of some micrometers from the interface is about 60 nm. This means that the thickness of the PnBMA film on top of PS is much larger than the performed deformations and, as a consequence, the mechanical properties of the sample probed by the cantilever are not affected by those of the underlying layer. Hence, the stiffening of PnBMA in the some tenths of a micrometer wide region near the interface cannot be explained only through the presence of any underlying PS. Much more, the effect of stresses resulting from the geometrical constraints close to the boundary turns to be essential to elucidate the spatial variations of the mechanical properties of PnBMA in the vicinity of the interface.

Moreover, eq 10 shows that, in presence of a double-layer sample, depending on the applied load, the elastic portion of the $D^{3/2}$ curves should compose of two lines. For $D \ll t^2/R$, i.e., for small loads, $D^{3/2}$ would tend to $D_H^{3/2}$, i.e., to the typical deformation on PnBMA, or, in other words, the $D^{3/2}$ curve would be a line with a slope γ as far away from the interface on PnBMA. Increasing the load, i.e., for $D \gg t^2/R$, $D^{3/2}$ would tend to $JD_H^{3/2}$, i.e., to the typical deformation on PS, or, in other words, the $D^{3/2}$ curve would be a line with a smaller slope γ, as on PS. Such a shape of the elastic part of the $D^{3/2}$ curves has never been seen. Rather, the elastic part of the $D^{3/2}$ curves is always a straight line. This confirms that the elastic deformations performed during force volume are too small to probe any underlying PS, and that the increase of Young's modulus of PnBMA near the interface is mainly due to the effect of stresses and not to the double-layer structure of the sample.

The detailed analysis of the $D^{3/2}$ curves on PnBMA close to the interface reveals the existence of another peculiarity of such curves with respect to the curves acquired far away from the interface. The plastic portion of the $D^{3/2}$ curves acquired near

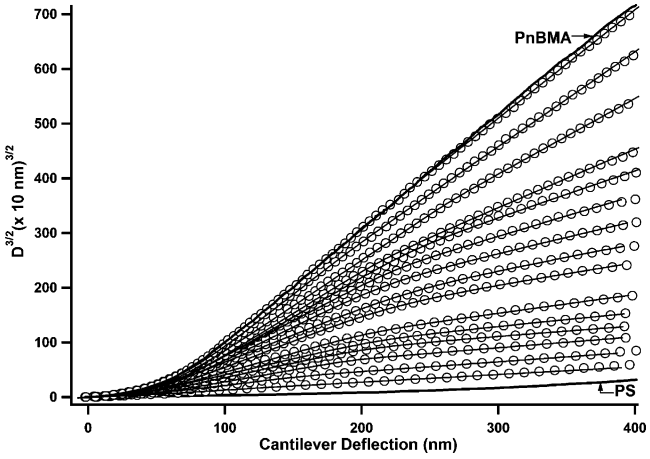

Figure 10. $D^{3/2}$ curves acquired at 57.4 °C on PnBMA at increasing distance from the interface (empty circles). Only one in eight points are shown for sake of clarity. The distances from the interface, from bottom to top, are: 0.8, 1.6, 2.4, 3.2, 4, 4.8, 6.4, 7.2, 8, 9.6, 10.4, 14.4, 16, 17.6, and 20.8 μm. Also the $D^{3/2}$ curves on PS and on PnBMA far from the interface are shown. The curve acquired at 21.6 μm from the interface overlaps the curve on PnBMA away from the interface. The continuous lines represent the fit with eq 11.

the interface is not proportional to the force, like in the curves acquired far from the interface (see Figure 3 and 4). Figure 10 shows several $D^{3/2}$ curves acquired at 51.4 °C on PnBMA at increasing distance from the interface (from 0.8 to 4.8 μm in steps of 800 nm, followed by the curves at 6.4, 7.2, 8, 9.6, 10.4, 14.4, 16, 17.6, and 20.8 μm from the interface), together with the $D^{3/2}$ curves on PS and on PnBMA far from the interface. Besides the deviation from the linear behavior in the plastic region (but not in the elastic region!), one can observe that such deviations become smaller and smaller with increasing distance from the interface, and that the curves gradually pass from a typical PS curve to a typical PnBMA curve, with the curve acquired at 21.6 μm from the interface overlapping the curve far away from the interface.

The deviations from the linear behavior for $F > F_{yield}$ are attributed both to the internal stresses induced in PnBMA at the boundary with PS and to the presence of the underlying PS layer. As a matter of fact, plastic deformations are performed at higher loads than elastic deformations, and they are so large, that an effect of underlying PS on the measured curves cannot be excluded, since at higher loads the tip probes a larger volume of the sample. It is of fundamental importance to remember that probing of the underlying PS layer by the tip does not imply that the deformations are as deep as the PnBMA layer on the top. As a matter of fact, as also in the Tsukruk model, the underlying layer is probed already at a deformation about 10 times smaller than the thickness of the upper layer.

Such deviations from the linear behavior hindered us from fitting the whole $D^{3/2}$ curves with a hyperbola as in eq 6, but they could be fitted with the following equation:

$$D^{3/2} = (\beta_1\delta_c - \epsilon_1) + \sqrt{\alpha_1^2\delta_c^2 - 2\epsilon_1(\beta_1 - \gamma_1)\delta_c + \epsilon_1^2} - (\beta_2\delta_c - \epsilon_2) - \sqrt{\alpha_2^2\delta_c^2 - 2\epsilon_2(\beta_2 - \gamma_2)\delta_c + \epsilon_2^2} \quad (11)$$

Equation 11 represents a hyperbola as in eq 6, to which, starting from a point $\delta^* = \epsilon_2/\alpha_2$, a second hyperbola is subtracted. Hence, the plastic regime is a composition of two lines.

The phenomena involved in the indentation of the sample near the boundary with PS can be summarized as follows. During the elastic indentation, deformations are influenced by the underlying PS only very close to the interface, i.e., in a narrow stripe, about 1 μm wide, or in other words only for the first two or three points after the interface in the images in Figure 7. At larger distances the cantilever probes only the upper PnBMA layer, that is much thicker than the performed indentation. The PnBMA near the interface (in a region going from some micrometers at 32 °C up to more than 60 μm at 70.1 °C) is stiffer than far from the interface. This is due to internal stresses arising from the geometrical constraints at the boundary with PS and from the tendency of PnBMA to dewet the stiff PS phase. Owing to such internal stresses, Young's modulus, inversely proportional to the slope of the elastic linear region, decreases from the PS value to the PnBMA value with increasing distance from the interface. Also the beginning of the plastic region is influenced by the internal stresses. By increasing the force, and hence the deformation, near the interface the AFM tip probes more and more the underlying PS. Since PS is in the glassy state, it is stiffer and harder than PnBMA, and, at a certain load, the plastic deformation on PS is smaller than on PnBMA. Furthermore, PS chains are not free to move like PnBMA chains, and cannot be squeezed out from the contact volume. Hence, starting from the load at which the probed volume includes also the underlying PS, the first derivative of the plastic region decreases, indicating that the resistance to plastic deformations is larger than in the PnBMA upper layer. At very high loads, the slope of the plastic region in the curves acquired in the several micrometers wide transition region in the vicinity of the boundary approaches the slope of the plastic region in the curves acquired on PS. Hence, the curves in the transition region are characterized by a "three-regimes" dependence on the force: the elastic region, influenced by internal stresses, a first plastic region, also influenced by internal stresses, and a second plastic region, influenced by the presence of underlying PS.

Since the thickness of PnBMA on the top of PS increases linearly with the distance from the interface, both effects of internal stresses and of underlying PS decrease with increasing distance from the interface. Hence, both the elastic region and the first plastic region become more and more similar to those of curves acquired on PnBMA far from the interface, and the second plastic region becomes shorter and shorter, until it disappears at a distance of about 20 μm from the interface.

Conclusions

We have exploited the high lateral resolution of force−displacement curves in determining the local mechanical properties of polymers as a function of temperature. The most important result of the present work is the quantitative determination of the dependence of Young's modulus of the components of a model polymer blend as a function of temperature using AFM force−displacement curves. Also, we have shown for the first time that the temperature-dependent Young's modulus calculated from the force−displacement curves can be used to map the morphology of the model blend.

It was possible to distinguish the two polymers at the interface taking advantage of the inherent difference in their T_g and of the resulting differences in their viscoelastic behavior. For the analysis of the deformations of the polymers, the proportionality between $D^{3/2}$ and δ_c, predicted by all elastic continuum contact theories, has been successfully employed in order to determine Young's modulus of the model blend. Thus, it is possible to characterize the temperature-dependent elastic properties of a two polymer model blend with a resolution of 800 nm, also in the vicinity of the interfacial region, using a novel analysis technique based on Hertz theory.

Young's moduli of the polymers have been compared with the results from DMA and AFM measurements shown in previous articles. In both cases there is a very good agreement between the measurements, proving the repeatability of the experiment and also the accuracy of the model used in calculating Young's modulus. Small differences between the several measurements are due to different preparation techniques.

The modulus of PS away from the interfacial region has been found to vary little over the entire experimental temperature range (from 10 GPa at 32 °C to 3.2 GPa at 70.1 °C), as PS was in its glassy state ($T_g = 100$ °C). In contrast, Young's modulus of PnBMA has been found to decrease steadily with increasing temperature (from 1.9 GPa at 32 °C to 0.08 GPa at 70.1 °C), as PnBMA turned rubbery ($T_g = 22$ °C).

The characterization of the mechanical properties of the model blend at the interface has shown the presence of a transition region, where Young's modulus decreases gradually from the value on PS to the value of PnBMA. The stiffening of PnBMA in such a transition region is attributed to internal stresses arising from the presence of a boundary with a stiff polymer for which PnBMA has no affinity to mixing. Such a hard wall boundary hinders the PnBMA phase to relax and expand and generates stresses that lead to an increase of the stiffness and of Young's modulus.

Since it was not possible to obtain a PS film with an absolutely sharp 90° edge, and the cut angle of PS was rather 20°, also the effect of a double-layer sample with a PnBMA film of increasing thickness on the top of the PS film must be accounted for. This effect has been found to be negligible for elastic deformations, since elastic deformations are much smaller than the thickness of PnBMA. On the contrary, in an approximately 20 μm wide region near the interface, plastic deformations, being larger than elastic deformations, are affected by the presence of underlying PS. An extension of our fitting model has been proposed for such curves.

References and Notes

(1) Briscoe, B.; Fiori, L.; Pelillo, E. *J. Phys. D* **1998**, *31*, 2395.
(2) Chizhik, S. A.; Huang, Z.; Gorbunov, V. V.; Myshkin, N. K.; Tsukruk, V. V. *Langmuir* **1998**, *14*, 2606.
(3) Reynaud, C.; Sommer, F.; Quet, C.; El Bounia, M.; Duc, T. M. *Surf. Interface Anal.* **2000**, *30*, 185.
(4) Raghavan, D.; Gu, X.; Nguyen, T.; VanLandingham, M. R.; Karim, A. *Macromolecules* **2000**, *33*, 2573.
(5) Du, B.; Tsui, O. K. C.; Zhang, Q.; He, T. *Langmuir* **2001**, *17*, 3286.
(6) Marti, O.; Stifter, T.; Waschipky, H.; Quintus, M.; Hild, S. *Colloids Surf. A* **1999**, *154*, 65.
(7) Tsui, O. K. C.; Wang, X. P.; Ho, J. Y. L.; Ng, T. K.; Xiao, X. *Macromolecules* **2000**, *33*, 4198.
(8) Bliznyuk, V. N.; Assender, H. E.; Briggs, G. A. D. *Macromolecules* **2002**, *35*, 6613.
(9) Cappella, B.; Kaliappan, S. K.; Sturm, H. *Macromolecules* **2005**, *38*, 1874.
(10) Kaliappan, S. K.; Cappella, B. *Polymer* **2005**, *46*, 11416.
(11) Paul, D. R.; Newman, S. In *Polymer Blends*; Academic Press: FL, 1974.
(12) Merfeld, G. D., Paul, D. R. In *Polymer Blend*; Paul, D. R., Bucknall, C. B., Eds.; Wiley: New York, 2000; Chapter 3.
(13) Djermouni, B.; Ache, H. J. *Macromolecules* **1980**, *13*, 168.
(14) Goldstein, J. I., Newbury, D. E., Chelin, P. E., Coy, D. C., Fiori, C.; Lifshin, C. In *Scanning Electron Microscopy and X-ray Microanalyses*; Plenum Press: New York, 1978.
(15) Sondergaard, K.; Lyngaae, J. *Polymer* **1986**, *37*, 509.
(16) Winnik, M. A. In *Photophysical and Photochemical Tools in Polymer Science: Conformation, Dynamic and Morphology*; NATO ASI Series; Reidel: Dordrecht, The Netherlands, 1986; Vol. 182.
(17) Sheiko, S. S. In *Advances in Polymer Science—Imaging of Polymers Using Scanning Force Microscopy*; Schmidt, M., Ed.; Springer-Verlag: Berlin and Heidelberg, Germany, 2000; Vol. 151.
(18) Cappella, B.; Dietler, G. *Surf. Sci. Rep.* **1999**, *34*, 1.
(19) Butt, H. J.; Cappella, B.; Kappl, M. *Surf. Sci. Rep.* **2005**, *59*, 1.
(20) Paige, M. F. *Polymer* **2003**, *44*, 6345.
(21) Noy, A.; Sanders, C. H.; Vezenov, D. V.; Wong, S. S.; Lieber, C. M. *Langmuir* **1998**, *14*, 1508.
(22) Magonov, S. N.; Elings, V.; Whangbo, M. H. *Surf. Sci.* **1997**, *375*, L385.
(23) Tsukruk, V. V.; Huang, Z. *Polymer* **2000**, *41*, 5541.
(24) Cappella, B.; Baschieri, P.; Frediani, C.; Miccoli, P.; Ascoli, C. *Nanotechnology* **1997**, *8*, 82.
(25) Radmacher, M.; Cleveland, P. J.; Fritz, M.; Hansma, H. G.; Hansma, P. K. *Biophys. J.* **1994**, *66*, 2154.
(26) Rotsch, Ch.; Radmacher, M. *Langmuir* **1997**, *13*, 2825.
(27) Dupont-Gillain, C. C.; Nysten, B.; Hlady, V.; Rouxhet, P. G. *J. Colloid Interface Sci.* **1999**, *220*, 163.
(28) Eaton, P. J.; Graham, P.; Smith, J. R.; Smart, J. D.; Nevell, T. G.; Tsibouklis, J. *Langmuir* **2000**, *16*, 7887.
(29) Ludwig, M.; Dettmann, W.; Gaub, H. J. *Biophys. J.* **1997**, *72*, 445.
(30) Grandbois, M.; Dettmann, W.; Benoit, M.; Gaub, H. E. *J. Histochem. Cytochem.* **2000**, *48*, 719.
(31) Kim, J. H.; Park, S.; Kim, C. K.; *J. Polym. Sci., Part B: Polym. Phys.* **2000**, *38*, 2666.
(32) Hertz, H. *J. Reine Angew. Math.* **1881**, *92*, 156.
(33) Domke, J.; Radmacher, M. *Langmuir* **1998**, *14*, 3320.
(34) VanLandingham, M. R. *Microsc. Today* **1997**, *97*, 12.
(35) Maugis, D. *J. Colloid Interface Sci.* **1992**, *150*, 243.
(36) Johnson, K. L.; Greenwood, J. A. *J. Colloid Interface Sci.* **1997**, *192*, 326.
(37) Cappella, B.; Sturm, H.; Weidner, S. M.; *Polymer* **2002**, *43*, 4461.
(38) Williams, M. L.; Landel, R.; Ferry, J. D. *J. Am. Chem. Soc.* **1955**, *77*, 525.
(39) Tsukruk, V. V.; Sidorenko, A.; Gorbunov, V. V.; Chizhik, S. A. *Langmuir* **2001**, *17*, 6715.

MA061896G